Available online at www.sciencedirect.com
ScienceDirect
Trans. Nonferrous Met. Soc. China 22(2012) s729−s734
Transactions of Nonferrous Metals Society of China
www.tnmsc.cn

Synthesis and properties of Cr−Al−Si−N films deposited by hybrid coating system with high power impulse magnetron sputtering (HIPIMS) and DC pulse sputtering

Min Su KANG[1], Tie-gang WANG[1, 2], Jung Ho SHIN[3,4], Roman NOWAK5, Kwang Ho KIM[1, 3]

1. School of Materials Science and Engineering, Pusan National University, Busan 609-735, Korea;
2. State Key Laboratory of Corrosion and Protection, Institute of Metal Research, Chinese Academy of Sciences, Shenyang 110016, China;
3. National Core Research Center for Hybrid Materials Solution, Pusan National University, Busan 609-735, Korea;
4. Extreme Energy-Density Research Institute, Nagaoka University of Technology, Nagaoka, Niigata 940-2188, Japan;
5. School of Chemical Technology, Aalto University, Aalto 00076, Finland;

Received 21 May 2012; accepted 24 September 2012

Abstract: The CrN and Cr−Al−Si−N films were deposited on Si wafer and SUS 304 substrates by a hybrid coating system with high power impulse magnetron sputtering (HIPIMS) and a DC pulse sputtering using Cr and AlSi targets under N_2/Ar atmosphere. By varying the sputtering current of the AlSi target in the range of 0−2.5 A, both the Al and Si contents in the films increased gradually from 0 to 19.1% and 11.1% (mole fraction), respectively. The influences of the AlSi cathode DC pulse current on the microstructure, phase constituents, mechanical properties, and oxidation behaviors of the Cr−Al−Si−N films were investigated systematically. The results indicate that the as-deposited Cr−Al−Si−N films possess the typical nanocomposite structure, namely the face centered cubic (Cr,Al)N nano-crystallites are embedded in the amorphous Si_3N_4 matrix. With increasing the Al and Si contents, the hardness of the film first increases from 20.8 GPa for the CrN film to the peak value of 29.4 GPa for the $Cr_{0.23}Al_{0.14}Si_{0.07}N$ film, and then decreases gradually. In the meanwhile, the $Cr_{0.23}Al_{0.14}Si_{0.07}N$ film also possesses excellent high-temperature oxidation resistance that is much better than that of the CrN film at 900 or 1000 °C.

Key words: Cr−Al−Si−N film; high power impulse magnetron sputtering; DC pulsed sputtering; high-temperature oxidation resistance

1 Introduction

Transition metal nitride coatings, such as TiN and CrN, were applied as hard coatings because of their high hardness, excellent wear resistance and chemical stability [1−5]. Among them, chromium nitride (CrN) coatings were widely used as protective coatings for various tribological forming and casting applications [6,7] because the coatings have high hardness as well as good wear resistance due to their low friction coefficients. CrN coatings also show excellent corrosion resistance under severe environmental conditions [8] and good oxidation resistance [9]. Recently, ternary Cr−X−N coatings, where X is the alloying element such as Ti [10,11], Al [12,13], Si [14,15], B [16], C [17,18], Ta [19,20], Nb [21], and Ni [22], have been actively investigated to improve the properties of CrN coatings. Among these ternary systems, Cr–Al–N films have higher hardness (25−32 GPa) than CrN coatings, and have much improved oxidation resistance up to 900 °C due to the formation of stable oxidation barrier of Al_2O_3 layer by migrated Al atoms to surface region [23,24]. Besides, Cr−Si−N coatings with nanocomposite structure consisting of nanosized CrN crystallites and amorphous SiN_x phase were also explored [15,25] to improve the hardness and tribological properties. More recently, quaternary Cr−Al−Si−N coatings started to be explored since it could become multi-functional coatings having superhardness (≥40 GPa), as well as excellent oxidation and wear resistance. However, relatively few research focused on Cr−Al−Si−N films was carried out [26−28],

Corresponding author: Kwang Ho KIM; Tel: +82-51-510-3391; E-mail: kwhokim@pusan.ac.kr
DOI: 10.1016/S1003-6326(12)61795-6

especially the study on their high-temperature oxidation resistance. It may be partly attributed to the difficulty in preparing dense Cr−Al−Si−N films. For instance, both AlN and CrN exhibit less electrical conductivity than TiN, which leads to microarcs caused by the charge accumulation [26]. The arcing phenomena severely degrade the quality of the film, even destroy some electrical components of the controlling system [29].

In this work, Cr−Al−Si−N films were synthesized by a hybrid coating system with a high power impulse magnetron sputtering (HIPIMS) [30,31] using Cr source and a DC pulse sputtering using AlSi source. The influence of the AlSi cathode DC pulse current on the chemical compositions, phase constituents, and mechanical properties of the films was investigated systematically. Moreover, the high-temperature oxidation resistance of the films was further evaluated.

2 Experimental

2.1 Film deposition

Cr−Al−Si−N films were deposited by a hybrid coating system combining an HIPIMS (Hauzer Techno Coating BV) and a DC pulse sputtering system as schematically shown in Fig. 1. The experiments were performed using an HIPIMS with Cr target and a pulse DC with AlSi target. The relative contents of Cr and AlSi can be controlled by adjusting the pulse DC power of AlSi target. A rotating sample holder was located at the center of vacuum chamber, about 100 mm from the targets. A bias power supply was connected to the sample holder. SUS 304 stainless steel material and Si wafers (for XRD, EPMA, TEM, residual stress analysis and oxidation test) were used as substrates. And then, all the substrates were ultrasonically cleaned in acetone and ethyl ethanol sequentially for 30 min, and fixed on the holder after being blown dry by pure nitrogen. The chamber was evacuated to a base pressure below 5.0×10^{-3} Pa using a rotary and turbo molecule pump. Before deposition, plasma etching was conducted by Ar glow discharge for 5 min with a DC bias of −700 V at 3.0×10^{-1} Pa. Then, ion bombardment was also conducted by the HIPIMS and the discharge of the Cr target for 5 min with a DC bias of −400 V at 3.2×10^{-1} Pa. To improve the adhesion between the film and the substrate, Cr and CrN layers were deposited for 5 min, respectively. The working pressure was maintained at 3.0×10^{-1} Pa and the volume ratio of reactive gas N_2 to inert gas Ar was kept at 2:1. The frequency of HIPIMS and duty cycle of the DC pulse power were maintained at 30 Hz and 50%, respectively. To keep other parameters constant, the DC pulsed power varied from 0 to 2.5 A to study its effect on the film microstructure and properties. The deposition time was 240 min and the deposition temperature was maintained at about 300 °C. The sample holder rotated continuously at 1000 r/min during the deposition process. The DC bias voltage was kept at −50 V, and no apparent micro-arcs were observed during all the deposition process.

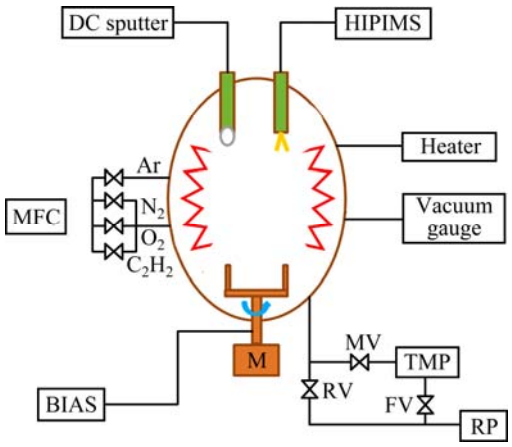

Fig. 1 Schematic diagram of hybrid coating system

2.2 Characterizations

The crystal structure of the films was determined by an X-ray diffractometer (XRD, D8-Discovery Brucker, Cu K_α, 40 kV, 40 mA). Diffraction patterns were collected from 20° to 80°. The surface and cross-section morphologies of the as-deposited and after oxidation test films were characterized by a scanning electron microscope (SEM, S 4800, Hitachi) coupled with an EDX accessory. The compositional analysis of the films was carried out using an electron probe microanalyzer (EPMA 1600, Shimadzu). The selected film was observed using a field emission transmission electron microscope (FE-TEM, JEOL, JEM−400FX) with an acceleration voltage of 400 kV. The hardness was evaluated by a microhardness tester with a Knoop indenter (Matsuzawa, MMT−7) under a load of 25 g.

3 Results and discussion

3.1 Chemical compositions and mechanical properties of Cr−Al−Si−N films

The Cr−Al−Si−N films with three different Al contents from 3.8% to 19.1% (mole fraction) and different Si contents from 1.8% to 11.1% (mole fraction), as well as the traditional CrN film were deposited, respectively. The chemical compositions of the above films determined by EPMA are shown in Fig. 2(a). Figure 2(b) shows the micro-hardness and residual stress of CrN and various Cr−Al−Si−N films deposited on Si wafer. All the Cr−Al−Si−N films show significantly higher hardness as compared with the CrN film. With the increase of the Al content to 13.5% and Si content to 7.1%, the film hardness increases gradually from 20.8 to

29.4 GPa. The above tendency is attributed to the grain boundary hardening phenomena created by strong cohesive energy of interphase boundaries [32] and by the Hall–Petch relation derived from crystal size refinement [33]. Both the formation of strong interphase boundaries and the refinement of crystallites result from the percolation of amorphous Si_3N_4 and SiO_2 phases into the grain boundaries of CrN and Cr−Al−N crystallites, respectively. Figure 2(b) also shows the residual stress graph plotted at various AlSi cathode DC pulse currents. All the films possess the compressive residual stress. With the increase of the AlSi cathode DC pulse current up to 1.5 A, the film residual stress increases gradually from −0.27 to −0.72 GPa. And then, the residual stress rebounds with further increase of the AlSi cathode DC pulse current. The reason of this phenomenon can be explained by the microstructural defects, which form due to the substitutional replacement of Al (R=1.43 Å) atoms for Cr (R=1.85 Å) sites in the films and play as a barrier to dislocation propagation.

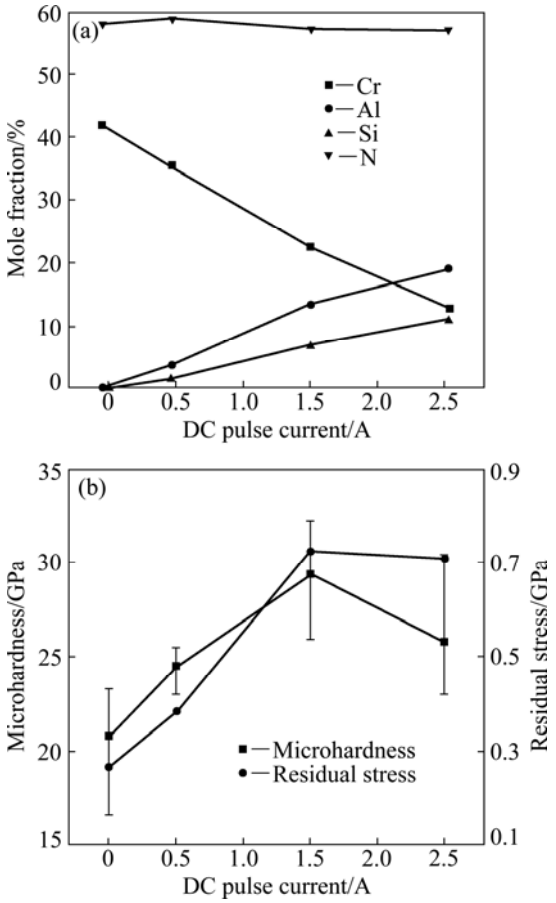

Fig. 2 EPMA results as function of DC pulse current (a) and microhardness and residual stress of Cr−Al−Si−N films as function of AlSi cathode DC pulse current (b)

3.2 Phase constituents and microstructure of Cr−Al−Si−N films

Figure 3 shows the XRD patterns of the Cr–Al–Si–N films deposited on Si wafer with various AlSi cathode DC pulse currents as well as the XRD pattern of the CrN film for comparison. The XRD peaks for the CrN film exhibit a pattern of the crystalline face-centered cubic (FCC) structure of CrN phase with orientations of (111), (200) and (113) crystal planes. The preferred growth direction of the crystal is (111). With the increase of the AlSi cathode DC pulse current, the peak intensity of (200) crystal plane increases rapidly and shows the significant preferred growth direction. As the element Al and/or Si is incorporated into the CrN film, the diffraction peak position shifts toward the higher angle compared with the XRD pattern of CrN film. Moreover, the above tendency becomes more obvious as the AlSi cathode DC pulse current is higher. These peak shift phenomena indicate that the added Al and Si can dissolve into CrN lattice by the substitutional replacement of Cr sites. Such an XRD peak broadening, in general, is an indication of either diminution of the grain size or the introduction of residual stress in the coating [34]. Any XRD peak corresponding to Cr_2N, Cr, Si_3N_4, $CrSi_2$, and AlN is not observed in Fig. 3.

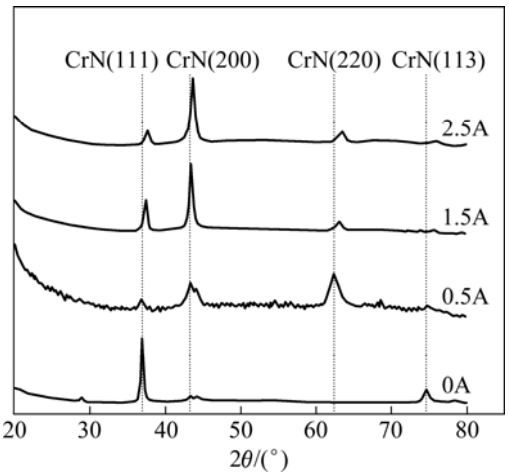

Fig. 3 XRD patterns of Cr−Al−Si−N films as function of AlSi cathode DC pulse current

In order to further investigate the microstructure of the Cr−Al−Si−N films, high resolution TEM observations were performed on the $Cr_{0.23}Al_{0.14}Si_{0.07}N$ film. Figure 4 shows the cross-sectional TEM images and selected area electron diffraction (SAED) pattern of the $Cr_{0.23}Al_{0.14}Si_{0.07}N$ film. From the bright field (BF) and dark field (DF) TEM images (Fig. 4(a)), it can be seen that the film possesses the columnar microstructure containing irregular nanograins. Figure 4(a) also presents the selected area electron diffraction pattern of the $Cr_{0.23}Al_{0.14}Si_{0.07}N$ film, which consists of the polycrystalline rings superimposed by diffraction spots that indicate the existence of the preferred growth orientation of crystals in the film [35]. The strong (111),

(200) and (220) rings are observed, which is consistent with the results in Fig. 3. Combining the results of XRD and SAED pattern, it can be inferred that Al exists in the form of (Cr, Al)N solid solution phase in the Cr–Al–Si–N films. Figure 4(b) shows the HRTEM image in the middle region of Fig. 4(a). It presents the typical nanocomposite structure consisting of the fine nanocrystallites and amorphous phase. These crystallites can be distinguished from each other by lattice fringe contrast. Meanwhile, the crystallites have irregular and ellipsoidal shapes, and do not fully homogeneously distribute in the amorphous phase.

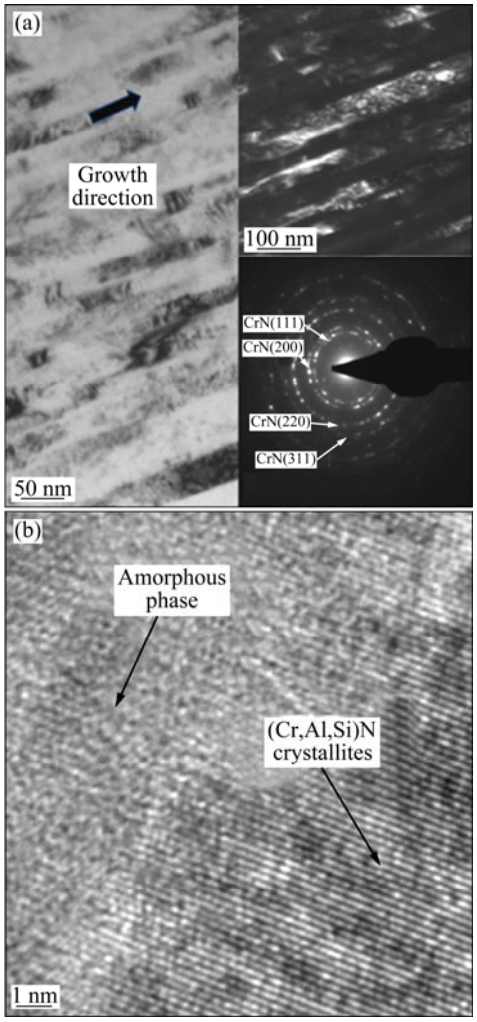

Fig. 4 BF-TEM, DF-TEM (with SAED) (a) and HR-TEM (with SAED) (b) images of $Cr_{0.23}Al_{0.14}Si_{0.07}N$ film

3.3 High-temperature oxidation resistance of Cr−Al−Si−N films

Figures 5(a) and (b) show the XRD patterns of the CrN and $Cr_{0.23}Al_{0.14}Si_{0.07}N$ films after oxidation test at 900 and 1000 °C in air for 1 h, respectively. From Fig. 5(a), it can be found that the XRD pattern of CrN film after oxidation test shows some new chromium oxide diffraction peaks besides the CrN peaks. Whereas

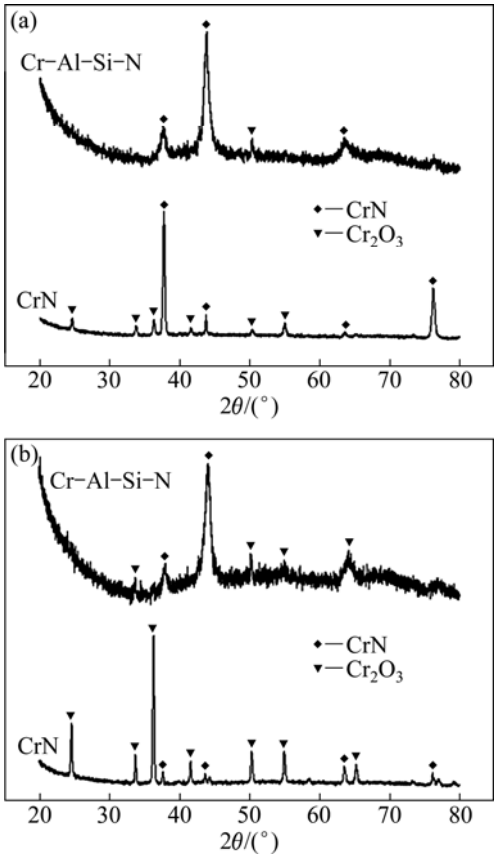

Fig. 5 XRD patterns of CrN and Cr−Al−Si−N films after oxidation test at 900 °C (a), and 1000 °C (b) in air for 1 h

in the XRD pattern of $Cr_{0.23}Al_{0.14}Si_{0.07}N$ film after oxidation test, almost no new diffraction peaks of oxide can be detected except for a weak peak at the angle of about 50°. To further heat up to 1000 °C, there are many diffraction peaks of oxide in the XRD pattern of CrN film (Fig. 5(b)), and the peak intensity also increases significantly compared with Fig. 5(a). However, in the XRD pattern of $Cr_{0.23}Al_{0.14}Si_{0.07}N$ film after oxidation test at 1000 °C, only some weak diffraction peaks of oxide appear.

Figure 6 shows the cross-sectional SEM images of the CrN and $Cr_{0.23}Al_{0.14}Si_{0.07}N$ films after the oxidation test. After oxidation test at 900 °C in air for 1 h, an apparent change happens for the microstructure of the CrN film. In Fig. 6(a), an oxide layer and loose columnar grains beneath the oxide layer exhibit on the fractured cross-section of the CrN film. On the other hand, the $Cr_{0.23}Al_{0.14}Si_{0.07}N$ film after oxidation at 900 °C still keeps the dense columnar structure without visible change. No apparent oxide layer is observed for the $Cr_{0.23}Al_{0.14}Si_{0.07}N$ film. As shown in Fig. 6(c), the oxidation of the CrN film becomes more severe at 1000 °C for 1 h than that at 900 °C. The oxide layer on the CrN film surface is thickened, whereas still no apparent oxide layer forms on the $Cr_{0.23}Al_{0.14}Si_{0.07}N$ film. The

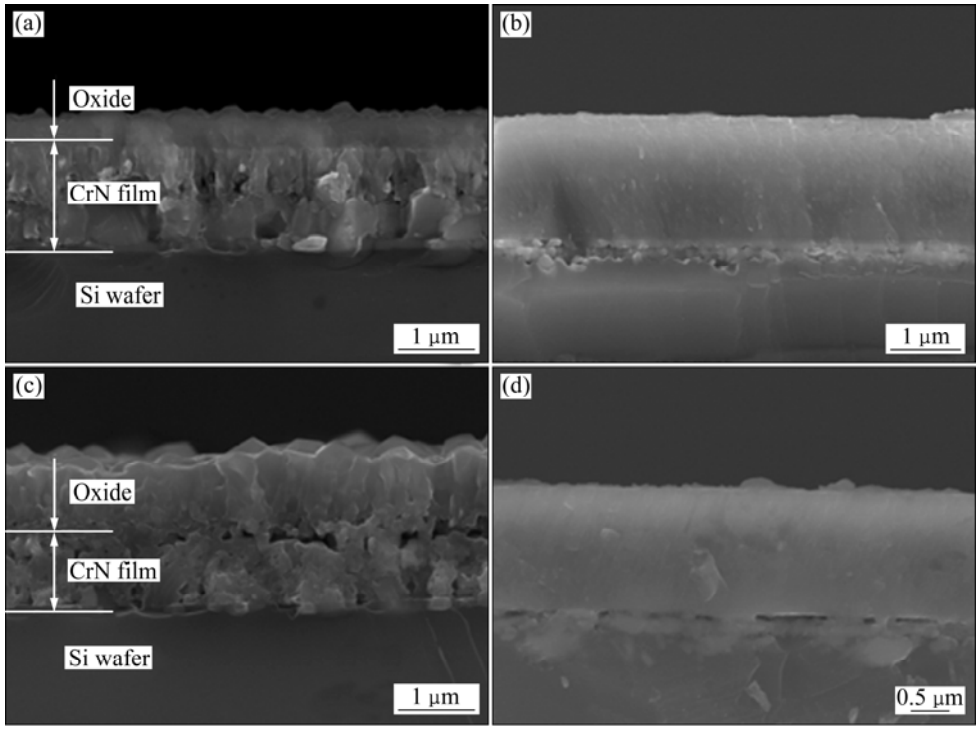

Fig.6 Cross-sectional SEM images of CrN (a,c) and Cr−Al−Si−N (b,d) films after oxidation test at 900 °C (a,b), 1000 °C (c,d) in air for 1 h

above phenomena indicate that the $Cr_{0.23}Al_{0.14}Si_{0.07}N$ film has much better oxidation resistance than that of the CrN film.

4 Conclusions

1) The CrN film and quaternary Cr−Al−Si−N films were deposited on SUS 304 stainless steel substrates and Si wafer by a hybrid coating system with HIPIMS and DC pulse magnetron sputtering using Cr and AlSi targets, respectively. The chemical compositions, microstructure, mechanical properties, and oxidation resistance of the CrN and Cr–Al–Si–N films were investigated and compared.

2) The Cr−Al−Si−N films consist of nano-sized (Cr,Al)N crystallites embedded in an amorphous Si_3N_4 matrix. The $Cr_{0.23}Al_{0.14}Si_{0.07}N$ film presents a maximum hardness of about 29.4 GPa, which is attributed to the mechanisms of solid-solution hardening and strain hardening. Meanwhile, the $Cr_{0.23}Al_{0.14}Si_{0.07}N$ film possesses the highest compressive residual stress. During the oxidation tests at 900 and 1000 °C, the $Cr_{0.23}Al_{0.14}Si_{0.07}N$ film exhibits much better oxidation resistance than the CrN film.

Acknowledgment

This work was supported by a 2-Year Research Grant of Pusan National University, Korea.

References

[1] HE J W, BAI D D, XU K W, HU N S. Improving the anticorrosion and mechanical behaviour of PACVD TiN [J]. Surface and Coating Technology, 1995, 74−75: 387−393.

[2] SUNDGREN J E, JOHANSSON B O, KARLASSON S E, HENTZELL H T G. Mechanisms of reactive sputtering of titanium nitride and titanium carbide II: Morphology and structure [J]. Thin Solid Films, 1983, 105(4): 367−384.

[3] NIEDERHOFER A, NESLADEK P, MANNLING H D, MOTO K, VEPREK S, JILEK M. Structural properties, internal stress and thermal stability of nc-TiN/a-Si_3N_4, nc-TiN/$TiSi_x$ and nc-($Ti_{1-y}Al_ySix$)N superhard nanocomposite coatings reaching the hardness of diamond [J]. Surface and Coating Technology, 1999, 120−121: 173−178.

[4] ECHIGOYA J, LIU Z T, IMAMURA A, TAKATSU A. Transmission electron microscopy studies of growth and interface structure of chemically vapour deposited TiC and TiN films on WC/Co alloy substrates [J]. Thin Solid Films, 1991, 198: 293−300.

[5] WITTMER M, NOSER J, MELCHIOR H. Oxidation kinetics of TiN thin films [J]. Journal of Applied Physics, 1981, 52(11): 6659−6664.

[6] REBHOLZ C, ZIEGELE H, LEYLAND A, MATTEW A. Structure, mechanical and tribological properties of nitrogen-containing chromium coatings prepared by reactive magnetron sputtering [J]. Surface and Coating Technology, 1999, 115: 222−229.

[7] CREUS J, INDRISS H, MAZILLE H, SANCHETTE F, JACQUOT P. Improvement of the corrosion resistance of CrN coated steel by an interlayer [J]. Surface and Coating Technology, 1998, 107: 183−190.

[8] NAVINSEK B, PANJAN P, MILOSEV I. Industrial applications of CrN (PVD) coatings, deposited at high and low temperatures [J]. Surface and Coating Technology, 1997, 97: 182−191.

[9] NAVINSEK B, PANJAN P. Novel applications of CrN (PVD)

coatings deposited at 200 °C [J]. Surface and Coating Technology, 1995, 74−75: 919−926.

[10] ZENG X T. Unbalanced magnetron sputtered carbon composite coatings [J]. Journal of Vacuum Science & Technology A, 1991, 17(4): 1991−1995.

[11] NAINAPARAMPIL J J, ZABINSKI J S, KORENYI-BOTH A. Formation and characterization of multiphase film properties of (Ti−Cr)N formed by cathodic arc deposition [J]. Thin Solid Films, 1998, 333: 88−94.

[12] ULRICH S, SATTEL S. Influence of low energy ion implantation on mechanical properties of magnetron sputtered metastable (Cr,Al)N thin films [J]. Thin Solid Films, 2003, 437: 164−169.

[13] SÁNCHEZ-LÓPEZ J C, MARTÍNEZ-MARTÍNEZ D, LÓPEZ-CARTES C, FERNÁNDEZ A, BRIZUELA M, GARCÍA-LUIS A, OÑATE. Mechanical behavior and oxidation resistance of Cr(Al)N coatings [J]. Journal of Vacuum Science & Technology A, 2005, 23(4): 681−686.

[14] PARK J H, CHUNG W S, CHO Y R, KIM K H. Synthesis and mechanical properties of Cr−Si−N coatings deposited by a hybrid system of arc ion plating and sputtering techniques [J]. Surface and Coating Technology, 2004, 188−189: 425−430.

[15] MARTINEZ E, SANJINES R, KARIMI A, ESTEVE J, LÉVY F. Mechanical properties of nanocomposite and multilayered Cr–Si–N sputtered thin films [J]. Surface and Coating Technology, 2004, 180−181: 570−574.

[16] ROTHER B, KAPPL H. Effects of low boron concentrations on the thermal stability of hard coatings [J]. Surface and Coating Technology, 1997, 96(2−3): 163−168.

[17] ALMER J, ODEN M, HAKANSSON G. Microstructure, stress and mechanical properties of arc-evaporated Cr−C−N coatings [J]. Thin Solid Films, 2001, 385: 190−197.

[18] YAO S H, SU Y L. The tribological potential of CrN and Cr(C,N) deposited by multi-arc PVD process [J]. Wear, 1997, 212(1): 85−94.

[19] CEKADA M, PANJAN P, NAVINSEK B, CVELBAR F. Characterization of (Cr,Ta)N hard coatings reactively sputtered at low temperature [J]. Vacuum, 1999, 52(4): 461−467.

[20] SAHA R, INTURI R B, BARNARD J A. Structural and mechanical characterization of Cr−Ta−N hard coatings prepared by reactive magnetron sputtering [J]. Surface and Coating Technology, 1996, 82(1−2): 42−47.

[21] TAN J N, HSIEH J H. Deposition and characterization of (Nb,Cr)N thin films by unbalanced magnetron sputtering [J]. Surface and Coating Technology, 2003, 167(2−3): 154−160.

[22] REGENT F, MUSIL J. Magnetron sputtered Cr−Ni−N and Ti−Mo−N films: comparison of mechanical properties [J]. Surface and Coating Technology, 2001, 142−144: 146−151.

[23] KAWATE M, HASHIMOTO A K, SUZUKI T. Oxidation resistance of $Cr_{1-X}Al_XN$ and $Ti_{1-X}Al_XN$ films [J]. Surface and Coating Technology, 2003, 165(2): 163−167.

[24] BANAKH O, SCHMID P E, SANJINES R, LÉVY F. High-temperature oxidation resistance of $Cr_{1-x}Al_xN$ thin films deposited by reactive magnetron sputtering [J]. Surface and Coating Technology, 2003, 163−164: 57−61.

[25] MERCS D, BONASSO N, NAAMANE S, BORDES J M, CODDET C. Mechanical and tribological properties of Cr−N and Cr−SI−N coatings reactively sputter deposited [J]. Surface and Coating Technology, 2005, 200: 403−407.

[26] KNOTEK O, LOEFFLER F, SCHOLL H. Properties of arc-evaporated CrN and (Cr,Al)N coatings [J]. Surface and Coating Technology, 1991, 45(1−3): 53−58.

[27] LUGSCHEIDER E, BOBZIN K, HORNIG T H, MASES M. Investigation of the residual stresses and mechanical properties of (Cr,Al)N arc PVD coatings used for semi-solid metal (SSM) forming dies [J]. Thin Solid Films, 2002, 420−421: 318−323.

[28] BARSHILIA H C, DEEPTHI B, SELVAKUMAR N, JAIN A, RAJAM K S. Nanolayered multilayer coatings of CrN/CrAlN prepared by reactive DC magnetron sputtering [J]. Applied Surface Science, 2007, 253(11): 5076−5083.

[29] ANDERS A. Physics of arcing, and implications to sputter deposition [J]. Thin Solid Films, 2006, 502(1−2): 22−28.

[30] KOUZNETSOV V, MACAK K, SCHNEIDER J M, HELMERSSON U, PETROV I. A novel pulsed magnetron sputter technique utilizing very high target power densities [J]. Surface and Coating Technology, 1999, 122(2−3): 290−293.

[31] HELMERSSON U, LATTEMANN M, BOHLMARK J, EHIASARIAN A P, GUDMUNDSSON J T. Ionized physical vapor deposition (IPVD): A review of technology and applications [J]. Thin Solid Films, 2006, 513(1−2): 1−24.

[32] VEPREK S, REIPRICH S, SHIZHI L. Superhard nanocrystalline composite materials: The TiN/Si_3N_4 system [J]. Applied Physics Letter, 1995, 66(20): 2640−2642.

[33] LASALMONIE A, STRUDEL J L. Influence of grain size on the mechanical behaviour of some high strength materials [J]. Journal of Materials Science, 1986, 21: 1837−1852.

[34] DISERENS M, PATSCHEIDER J, LÉVY F. Improving the properties of titanium nitride by incorporation of silicon [J]. Surface and Coating Technology, 1998, 108−109: 241−246.

[35] KIM S K, VINH P V, LEE J W. Deposition of superhard nanolayered TiCrAlSiN thin films by cathodic arc plasma deposition [J]. Surface and Coating Technology, 2008, 202: 5395−5399.

(Edited by CHEN Wei-ping)